Article

Cell Reports

Distinct Corticostriatal GABAergic Neurons Modulate Striatal Output Neurons and Motor Activity

Graphical Abstract

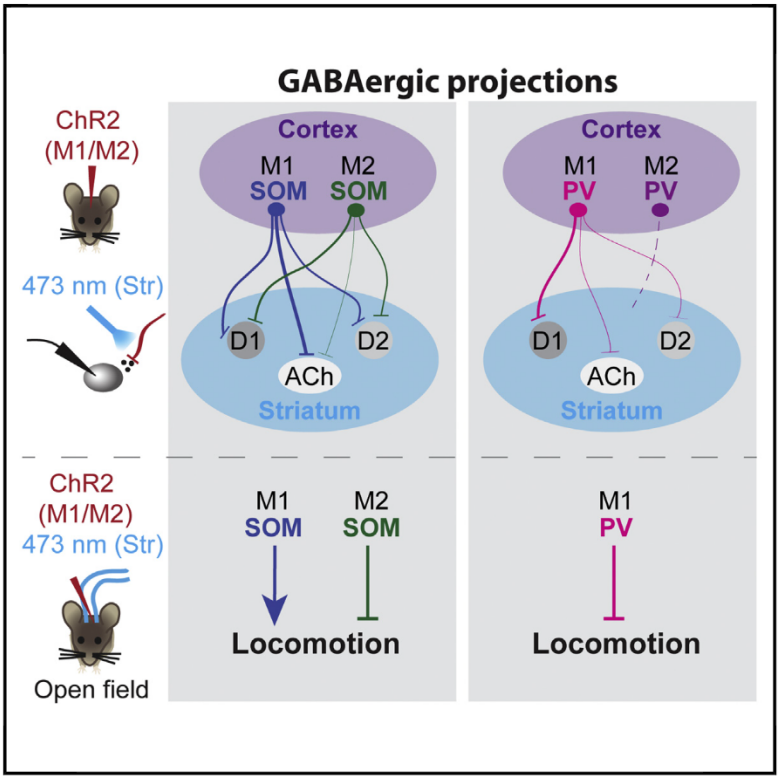

Authors

Sarah Melzer, Mariana Gil, David E. Koser, Magdalena Michael, Kee Wui Huang, Hannah Monyer

Correspondence

h.monyer@dkfz-heidelberg.de

In Brief

Melzer et al. characterize two cytochemically distinct GABAergic projecting neurons from the motor cortex to the dorsal striatum. These distinct populations of motor cortex GABAergic projecting neurons differentially innervate striatal neurons and differentially modulate motor activity.

Highlights

- Long-range GABAergic projections from the motor cortex directly innervate the striatum
- M1 and M2 long-range SOM$^+$ and PV$^+$ neurons differentially innervate striatal neurons
- Striatal cholinergic neurons are innervated mainly by M1 SOM$^+$ projecting neurons
- Motor cortex PV$^+$ and SOM$^+$ projecting neurons differentially modulate locomotion

Melzer et al., 2017, Cell Reports *19*, 1045–1055
May 2, 2017
http://dx.doi.org/10.1016/j.celrep.2017.04.024

Cell Reports
Article

Distinct Corticostriatal GABAergic Neurons Modulate Striatal Output Neurons and Motor Activity

Sarah Melzer,[1,3,4] Mariana Gil,[1,3] David E. Koser,[1] Magdalena Michael,[1] Kee Wui Huang,[2] and Hannah Monyer[1,5,*]
[1]Department of Clinical Neurobiology at the Medical Faculty of Heidelberg University and German Cancer Research Center (DKFZ), Im Neuenheimer Feld 280, 69120 Heidelberg, Germany
[2]Department of Neurobiology, Howard Hughes Medical Institute, Harvard Medical School, 220 Longwood Avenue, Boston, MA 02115, USA
[3]These authors contributed equally
[4]Present address: Department of Neurobiology, Howard Hughes Medical Institute, Harvard Medical School, 220 Longwood Avenue, Boston, MA 02115, USA
[5]Lead Contact
*Correspondence: h.monyer@dkfz-heidelberg.de
http://dx.doi.org/10.1016/j.celrep.2017.04.024

SUMMARY

The motor cortico-basal ganglion loop is critical for motor planning, execution, and learning. Balanced excitation and inhibition in this loop is crucial for proper motor output. Excitatory neurons have been thought to be the only source of motor cortical input to the striatum. Here, we identify long-range projecting GABAergic neurons in the primary (M1) and secondary (M2) motor cortex that target the dorsal striatum. This population of projecting GABAergic neurons comprises both somatostatin-positive (SOM$^+$) and parvalbumin-positive (PV$^+$) neurons that target direct and indirect pathway striatal output neurons as well as cholinergic interneurons differentially. Notably, optogenetic stimulation of M1 PV$^+$ and M2 SOM$^+$ projecting neurons reduced locomotion, whereas stimulation of M1 SOM$^+$ projecting neurons enhanced locomotion. Thus, corticostriatal GABAergic projections modulate striatal output and motor activity.

INTRODUCTION

The striatum is the primary input area of the basal ganglia. It integrates signals from cortical areas and subserves important functions like motor control (Tecuapetla et al., 2014; Kravitz et al., 2010) and reinforcement/punishment coding (Kravitz et al., 2012). Striatal neurons comprise GABAergic spiny projection neurons (SPNs, 95%) and interneurons (5%). SPNs are classified into direct pathway SPNs (dSPNs), which project to the substantia nigra reticulata and external and internal segments of the globus pallidus (GPe and GPi, respectively), and indirect pathway SPNs (iSPNs), which project to GPe (Bolam et al., 2000; Wu et al., 2000). Striatal interneurons include large aspiny cholinergic neurons and different populations of GABAergic interneurons (Kawaguchi et al., 1995).

Excitatory glutamatergic neurons from virtually all cortical areas send projections to the striatum (McGeorge and Faull, 1989), and several studies suggest their recruitment during action selection (Xiong et al., 2015; Znamenskiy and Zador, 2013; Koralek et al., 2012). In contrast, cortical GABAergic neurons projecting to the striatum were not considered to be a component of the canonical corticostriatal network because they were identified only in the prefrontal, somatosensory, and retrosplenial cortices (Lee et al., 2014; Jinno and Kosaka, 2004). Only recently were direct GABAergic neurons projecting to the striatum also described in the motor and auditory cortices (Rock et al., 2016). The authors identified the long-range projecting neurons as somatostatin-positive (SOM$^+$) and, furthermore, reported that inhibition conveyed by these neurons was onto both dSPNs and iSPNs. We previously showed that long-range GABAergic neurons connecting several brain structures comprise different molecular subtypes. For instance, connectivity between the hippocampus and medial entorhinal cortex is supported by parvalbumin-positive (PV$^+$) and SOM$^+$ neurons (Melzer et al., 2012). Moreover, projections from the septum to the medial entorhinal cortex are PV$^+$ and Calbindin$^+$, and they inhibit specific interneurons differentially (Fuchs et al., 2016). Hence, we wondered whether long-range GABAergic projecting neurons from the motor cortex to the striatum are diverse with respect to their molecular identity, target specificity, and function at the behavioral level.

Based on virus-mediated tracing, optogenetics, patch-clamp recordings in vitro, and behavioral essays, we identified two distinct populations of long-range projecting GABAergic neurons in the primary (M1) and secondary (M2) motor cortex targeting the dorsal striatum and established that these two populations exhibit target cell preference in the striatum and affect locomotion differentially.

RESULTS

Motor Cortex Long-Range Projecting SOM$^+$ Neurons Target the Striatum

SOM$^+$ cells are a major source of intracortical and corticofugal long-range GABAergic projections (Tomioka et al., 2005; Rock

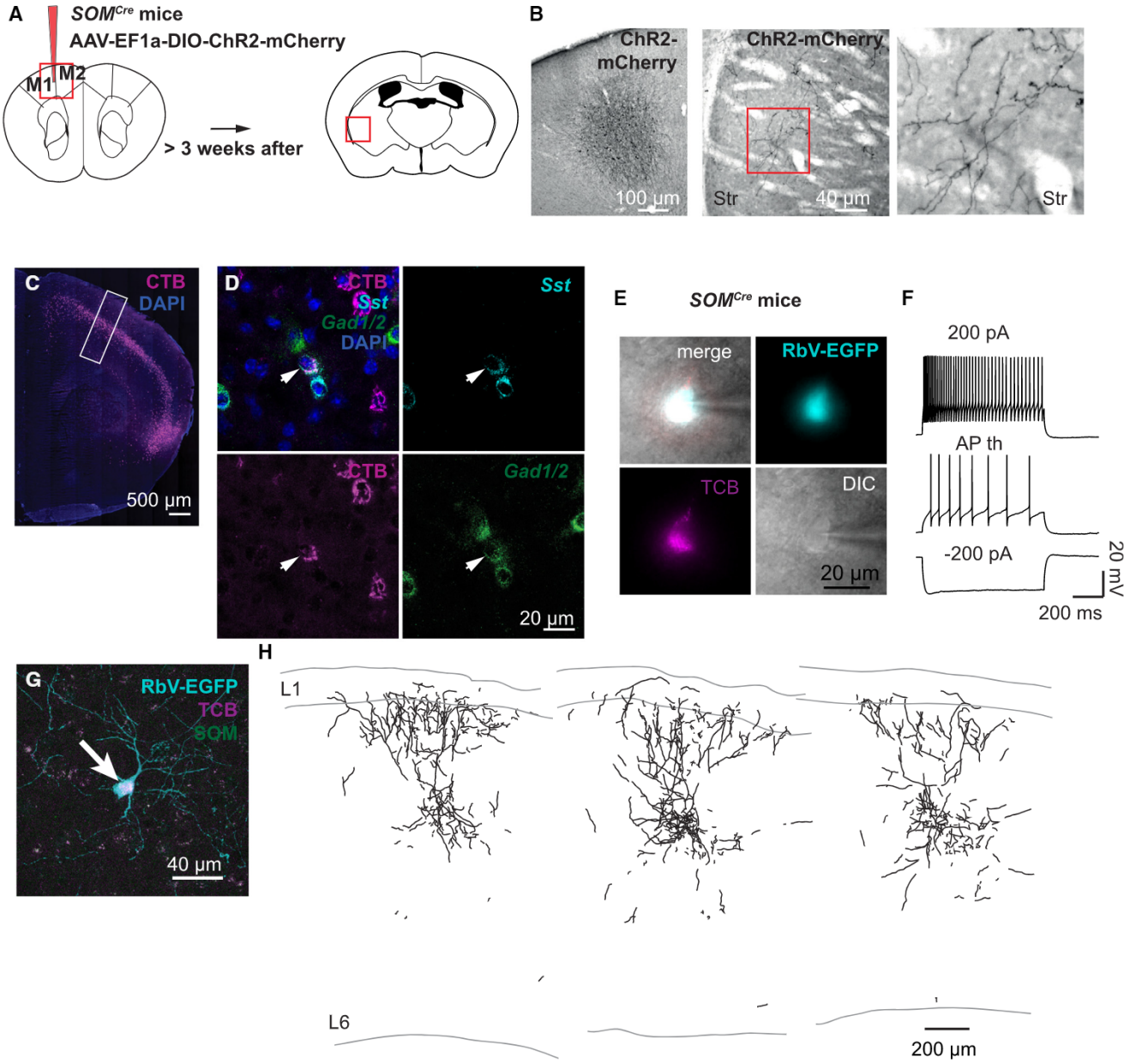

Figure 1. Motor Cortex SOM$^+$ GABAergic Neurons Innervate the Striatum

(A) Schematic drawing of the injection site and the location of long-range projections in the striatum shown in (B). Viral constructs encoding ChR2-mCherry were injected into the motor cortex of *SOM^{Cre}* mice.

(B) Bright-field images of DAB-stained sections showing the injection site in the motor cortex (left) and mCherry-labeled axons in the striatum (center) following AAV DIO *ChR2-mCherry* injection into the motor cortex of *SOM^{Cre}* mice. A higher magnification of the boxed area is shown on the right.

(C and D) Confocal images showing a retrogradely labeled area (C) following injection of the retrograde tracer CTB647 into the striatum and a retrogradely labeled GABAergic SOM$^+$ neuron in the motor cortex, visualized via FISH for *Sst* and *Gad1/2* (D).

(E–H) SOM$^+$ projecting neurons were identified by retrograde tracing with SADΔG-EGFP(EnvA) rabies virus. TCB was expressed Cre-dependently in the motor cortex of *SOM^{Cre}* mice, and rabies virus was injected into the striatum. (E) shows differential interference contrast (DIC) and epifluorescent images of a retrogradely labeled TCB$^+$ neuron in the motor cortex with the corresponding firing pattern shown in (F). (G) shows a confocal image of a retrogradely labeled TCB$^+$ neuron in M1 immunostained for EGFP and SOM with the corresponding morphological reconstruction shown in (H).

Str, striatum. See also Figure S1 and Tables S1 and S2.

et al., 2016). To substantiate and extend these studies focusing on long-range GABAergic neurons connecting the motor cortex and the striatum, we injected adeno-associated virus (AAV) double-floxed inverse open reading frame (DIO) *ChR2-mCherry* into the M1 and M2 area of *SOM^{Cre}* mice. This resulted in labeling of a subpopulation of GABAergic neurons (Figures 1A and 1B;

Figure S1A) and revealed projections in several ipsilateral cortical and subcortical areas and, to a lesser extent, in contralateral cortices (Table S1). There was consistent innervation of the ipsilateral dorsal striatum (Figure 1B; Table S1). Motor cortex SOM^+ neuron projections traversed the dorsal striatum and branched preferentially ventro-laterally, sparing the most rostral and caudal part of the dorsal striatum (Figure 1B).

To further substantiate the presence of GABAergic corticostriatal projections, we performed retrograde labeling. We injected cholera toxin B (CTB) subunit 647 into the ventro-lateral part of the dorsal striatum and analyzed retrogradely labeled cells in the M1 region (Figures S1B and S1C). As expected, a dense band of retrogradely labeled cells became visible in cortical L5 (Figure 1C); i.e., in the layer that is the major source of corticostriatal excitatory projections (Wilson, 1987; Cowan and Wilson, 1994). To visualize GABAergic cells among the M1 retrogradely labeled cells, we performed multi-fluorescence in situ hybridization (FISH) for *Sst* (encoding SOM) and *Gad1/2* (encoding GAD67/65). We found 13 retrogradely labeled cells in M1 that were clearly positive for *Gad1/2* (n = 3,582 CTB^+ cells and 5,064 $Gad1/2^+$ cells, cell counts across all layers in 35 slices from 4 hemispheres in 4 mice), 8 of which co-labeled for *Sst* (Figure 1D). Most retrogradely labeled GABAergic neurons were located in L5 (Figure S1D). To confirm a direct long-range GABAergic connection between the motor cortex (M1/M2) and the dorsal striatum, we performed retrograde monosynaptic tracing with rabies virus (Wickersham et al., 2007). We injected AAVs encoding Cre-dependent avian virus receptor (avian tumor virus receptor A mCherry [TCB]; Weissbourd et al., 2014) and rabies glycoprotein (RG) into the striatum of A2A-Cre mice that express Cre recombinase specifically in iSPNs (Gong et al., 2003). Subsequent injection of RG-deleted envelope protein from avian ASLV type A (EnvA)-pseudotyped rabies virus (SADΔG-EGFP(EnvA)) into the striatum resulted in transsynaptically retrogradely labeled cells in the cortex (Figures S1E and S1F). FISH for rabies virus-specific mRNA (*RabV-gp1*) and *Gad1/2* revealed double-positive neurons in the motor cortex (7 cells in 34 slices from 4 hemispheres in 4 mice; Figure S1G). The average number of labeled cells per slice was lower than after CTB647 injections, suggesting that iSPNs were not the only striatal target cells of GABAergic projecting neurons and/or reflecting lower efficiency of transsynaptic tracing (Marshel et al., 2010).

To determine the electrophysiological and morphological properties of SOM^+ projecting neurons, we expressed TCB Cre-dependently in the motor cortex (M1/M2) of SOM^{Cre} mice and injected SADΔG-EGFP(EnvA) rabies virus into the striatum. TCB^+ retrogradely labeled cells in the motor cortex had a classical or burst accommodating firing pattern (n = 11 cells from 5 hemispheres in 4 mice; Figures 1E and 1F; Figure S1H) similar to non-retrogradely labeled TCB^+ cells (Table S2). Reconstructed cells had a Martinotti cell-like morphology (Wang et al., 2004) with axonal projections extending over all cortical layers (three reconstructions from three hemispheres in two mice; Figures 1G and 1H; Figures S1I–S1K).

Motor Cortex Long-Range Projecting SOM^+ Neurons Differentially Inhibit Striatal Neurons

We next tested whether SOM^+ projecting neurons form functional synapses onto striatal neurons and whether the connectivity exhibits target specificity. We injected AAV DIO *ChR2-mCherry* into M1/M2 of SOM^{Cre} mice and combined optogenetic stimulation of long-range projections with patch-clamp recordings of putative postsynaptic cells in the striatum (Figure 2A). All injections (n = 36 hemispheres) resulted in labeled axons that projected to the dorsal striatum. Patched neurons were selected to be in close proximity to labeled axons. Of 305 patched neurons (in 27 mice), 50 responded with short-latency postsynaptic currents (PSCs) to 5-ms photostimulation of motor cortex SOM^+ neuron projections (Figure 2B). As a specificity control, we repeated the experiment in wild-type mice injected with AAV DIO *ChR2-mCherry* and found neither $mCherry^+$ fibers in the dorsal striatum nor a response after photostimulation (n = 58 cells in 2 mice). Responses in SOM^{Cre} mice could not be blocked with 6-cyano-2,3-dihydroxy-7-nitro-quinoxaline (CNQX) and D-2-Amino-5-Phosphonovaleric acid (D-AP5) (165.6 ± 32.7 pA baseline versus 169.5 ± 31.1 pA with drugs [mean ± SEM], paired t test, $t_{(14)} = 0.49$, p = 1, n = 15 cells in 11 mice; Figure S2A) but with gabazine (117.8 [134.3] pA versus 1.6 [1.6] pA [median interquartile range (IQR)], Wilcoxon signed-rank test, W = 210, p = 0.0002, n = 20 cells in 15 mice; Figures S2A and S2B). Responses reversed around the reversal potential of GABAergic receptors (n = 14 cells in 9 mice; Figure 2B), thus confirming the GABAergic nature of motor cortex SOM^+ neuron projections.

To scrutinize target specificity, striatal neurons were sorted into SPNs and cholinergic and GABAergic interneurons based on their electrophysiological properties and cell soma shape (Planert et al., 2013; Gertler et al., 2008; Kawaguchi, 1992; Bennett and Wilson, 1999; Kawaguchi et al., 1995; Experimental Procedures; Figures 2C–2E; Table S3). We found that 22.6% of SPNs, 33.3% of cholinergic cells, and only 2% of GABAergic interneurons responded to 5-ms photostimulation of motor cortex SOM^+ neuron projections (Figure 2F; Figures S2C and S2D; Table S3). Together, these data indicate that SPNs and cholinergic cells are the main target of motor cortex SOM^+ neuron projections.

To answer whether dSPNs and iSPNs are differentially targeted by motor cortex SOM^+ projecting neurons, we crossbred SOM^{Cre} mice to DRD1a-EGFP and DRD2-EGFP mice in which dSPNs and iSPNs, respectively, are selectively labeled (Gong et al., 2003; Figures 2G and 2H). Furthermore, we tested for differential innervation from M1 and M2. We injected AAV DIO *ChR2-mCherry* into M1 or M2 of SOM^{Cre}/DRD1a-EGFP or SOM^{Cre}/DRD2-EGFP mice (Figure 2G; Figure S2E) and combined photostimulation of M1 or M2 SOM^+ neuron projections with patch-clamp recordings of striatal neurons (Figure S2F). We found that M1 SOM^+ projecting neurons innervated a comparable proportion of dSPNs (29%), iSPNs (22%), and cholinergic cells (40%) (Figures 2I and 2J; Fisher's exact test, p = 0.19). M2 SOM^+ projecting neurons targeted dSPNs (25%) and iSPNs (16%) to a similar extent, whereas cholinergic cells tended to be innervated less frequently (4%) (Figure 2J; Fisher's exact test, p = 0.08). Inhibition of cholinergic cells by M2 was significantly less frequent than by M1 (Figure 2J; Fisher's exact test, M1 dSPNs versus M2 dSPNs: p = 1; M1 iSPNs versus M2 iSPNs: p = 1; M1 cholinergic versus M2 cholinergic: p = 0.006). Responses had a latency of 2.5 (1.3) ms (median [IQR]; n = 47

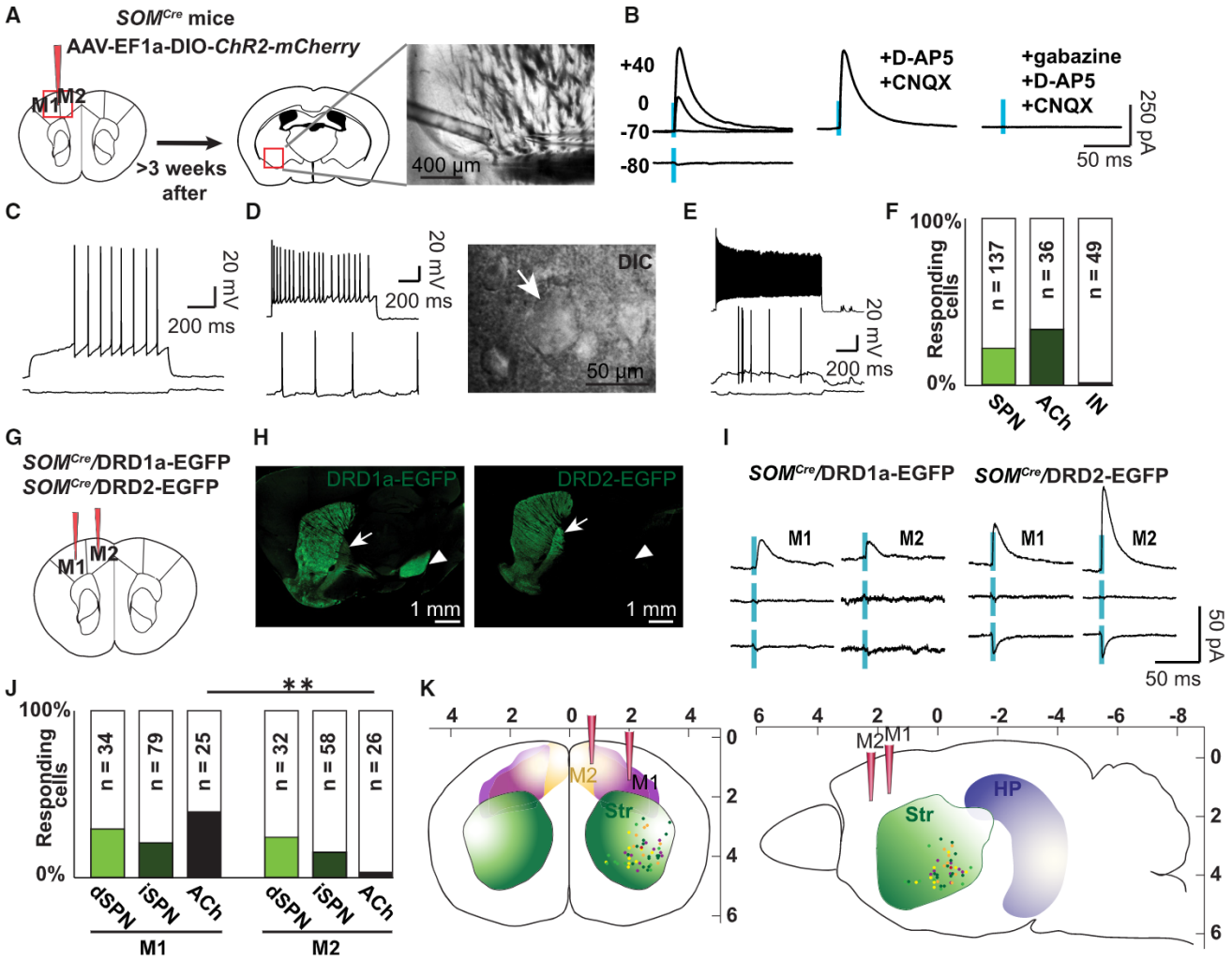

Figure 2. Motor Cortex SOM$^+$ Neuron Projections Form Functional Synapses on Striatal Output and Cholinergic Neurons

(A) Schematic drawing indicating the injection site (left) and location of an exemplary patched neuron in the striatum (right). AAV DIO *ChR2-mCherry* was injected into the motor cortex of *SOM^{Cre}* mice, and target cells were patched in the striatum (DIC image).

(B) PSCs recorded in a striatal neuron at the indicated holding potentials following 5-ms photostimulation (blue ticks) of motor cortex SOM$^+$ neuron projections. Responses were blocked with gabazine but not D-AP5/CNQX.

(C) Firing pattern (membrane potential upon −50-pA current injection and at the action potential [AP] threshold) of a representative SPN that was responsive to photostimulation of motor cortex SOM$^+$ neuron projections.

(D) Firing pattern (spontaneous activity and maximal firing frequency) and DIC image of a representative cholinergic interneuron (arrow) that was responsive to photostimulation of motor cortex SOM$^+$ neuron projections.

(E) Firing pattern of a striatal GABAergic interneuron that was responsive to photostimulation of motor cortex SOM$^+$ neuron projections (from top to bottom: maximal firing frequency, AP threshold, and −50-pA current injection).

(F) Percentage of striatal neurons responding to photostimulation of motor cortex SOM$^+$ neuron projections. The numbers in the bars indicate the total number of patched cells. Number of mice: SPNs, 19; cholinergic, 11; GABAergic interneurons, 19.

(G) Schematic drawing indicating injection sites of AAV DIO *ChR2-mCherry* in *SOM^{Cre}*/DRD1a-EGFP and *SOM^{Cre}*/DRD2-EGFP mice.

(H) Confocal image of EGFP-immunostained sagittal sections of *SOM^{Cre}*/DRD1a-EGFP (left) and *SOM^{Cre}*/DRD2-EGFP (right) mice exhibiting differential EGFP expression in the globus pallidus (arrow) and substantia nigra (arrowhead).

(I) Exemplary traces of dSPN and iSPN responses to photostimulation (blue ticks) of M1 and M2 SOM$^+$ neuron projections using Cs^+-based low Cl^- intracellular solution (from top to bottom: 0 mV, reversal potential, and −95 mV holding potential).

(J) Percentage of striatal neurons responding to photostimulation of M1 and M2 SOM$^+$ neuron projections. The numbers in the bars indicate the total number of patched cells. Number of mice: M1-dSPNs, 7; M1-iSPNs, 16; M2-dSPNs, 8; M2-iSPNs, 17; M1-cholinergic, 19; M2-cholinergic, 13.

(K) Schematic drawing indicating the localization of responding cells in a coronal (left) and sagittal (right) cross-section. Color code: orange, M1 to dSPN; yellow, M2 to dSPN; dark green, M1 to iSPN; light green, M2 to iSPN; purple, M1 to cholinergic interneuron; red, M2 to cholinergic interneuron.

HP, hippocampus; ACh, cholinergic interneuron. See also Figures S2 and S3 and Tables S3 and S4.

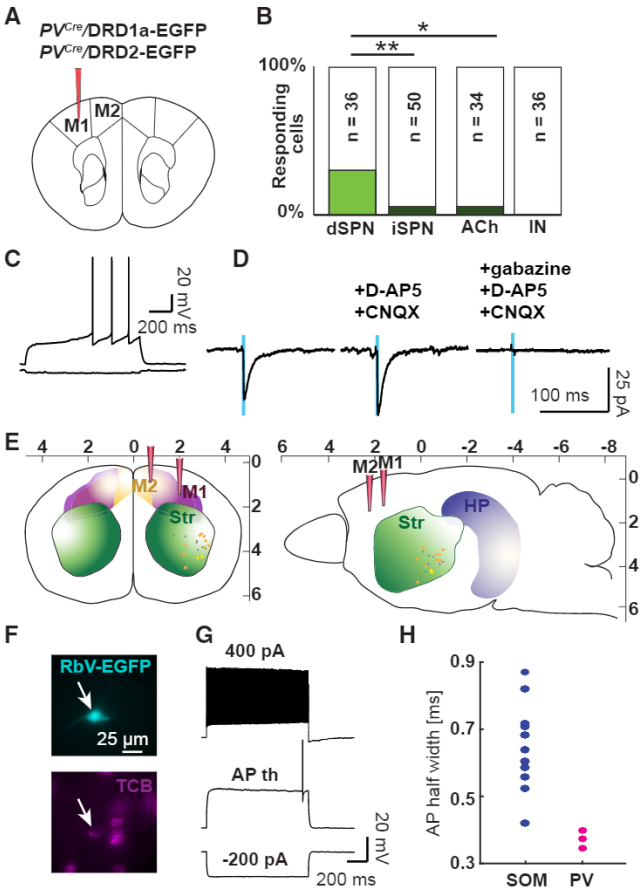

Figure 3. M1 PV$^+$ Neuron Projections Preferentially Target dSPNs in the Striatum

(A) Schematic drawing indicating the injection site of AAV DIO *ChR2-mCherry* in *PV^{Cre}*/DRD1a-EGFP and *PV^{Cre}*/DRD2-EGFP mice.

(B) Percentage of striatal neurons responding to photostimulation of M1 PV$^+$ neuron projections. The numbers indicate the total numbers of patched cells. Number of mice: dSPNs, 8; iSPNs, 7; cholinergic, 13; GABAergic interneurons, 9.

(C) Firing pattern (upon −50 pA current injection and at the AP threshold) of a representative dSPN that was responsive to photostimulation of M1 PV$^+$ neuron projections.

(D) Responses of the dSPN shown in (C) at −70 mV holding potential using high Cl$^-$ intracellular solution. Responses were blocked with gabazine but not D-AP5/CNQX.

(E) Schematic drawing indicating the localization of responding cells in a coronal (left) and sagittal (right) cross-section. Color code: orange, M1 to dSPN; yellow, M1 to iSPNs; gray, unidentified responding neurons.

(F and G) Epifluorescent images of a retrogradely labeled TCB$^+$ neuron in the motor cortex (arrow) (F) with the corresponding firing pattern (G) identified by retrograde tracing with SADΔG-EGFP(EnvA) rabies virus. TCB was expressed Cre-dependently in the motor cortex of *PV^{Cre}* mice, and rabies virus was injected into the striatum.

(H) Dot plot of the action potential half-width for retrogradely labeled SOM$^+$ (n = 11 cells from 5 hemispheres in 4 mice) and PV$^+$ neurons (n = 3 cells from 3 hemispheres in 2 mice).

See also Figure S3 and Tables S2 and S4.

responding cells; see Figure S3A and Table S4 for more details) and a reversal potential of −58.0 ± 1.4 mV (mean ± SEM; n = 22 responding cells; see Figure S3B and Table S4 for more details).

The strength of M1 and M2 SOM$^+$ neuron connections to SPNs was similar (Table S4). However, when comparing inputs with dSPNs and iSPNs both from M1 and M2, the response amplitudes were significantly larger for iSPNs (amplitudes at 0 mV with cesium [Cs$^+$] internal solution: 15.7 [29] pA versus 44.0 [36.5] pA [median (IQR)] in dSPNs and iSPNs respectively; Mann-Whitney *U* test, U = 102, p = 0.02, n = 14 and 26 responding cells, respectively; Figure S3C). Detected target cells were located preferentially in the ventro-lateral part of the dorsal striatum (Figure 2K; Figures S3D–S3F; Table S4). Targeted dSPNs and iSPNs were intermingled and localized 2.4 (0.7) mm lateral, 0.1 (0.7) mm posterior to the bregma and 4 (0.7) mm deep (median [IQR]). SPNs targeted by M1 projections were more lateral than SPNs targeted by M2 projections (Mann-Whitney *U* test, U = 142, p = 0.04; Table S4).

Motor Cortex Long-Range Projecting PV$^+$ Neurons Differentially Inhibit Striatal Neurons

The retrograde labeling experiments suggested that SOM$^+$ neurons are not the only M1 GABAergic population projecting to the striatum. PV$^+$ neurons appeared to be attractive candidates because we identified them before as a major class of neurons providing long-range inhibition in the entorhinal cortex-hippocampal formation (Melzer et al., 2012). Testing for the presence of GABAergic long-range projecting PV$^+$ cells based on virus tracing in *PV^{Cre}* mice may be complicated by the fact that a fraction of cortical PV$^+$ cells are glutamatergic (Jinno and Kosaka, 2004). Hence, we first tested the GABAergic nature of PV$^+$ cells in M1/M2 by counting the number of double-positive cells in injected *PV^{Cre}*/*GAD67^{EGFP}* mice. 99.5% of PV$^+$ cells were GAD67$^+$ (759 of 763 PV$^+$ cells from 9 slices in 3 mice). This result is in agreement with previous evidence showing the absence of PV$^+$ glutamatergic neurons in the motor cortex (Jinno and Kosaka, 2004). In the mouse neocortex, PV$^+$ and SOM$^+$ neurons constitute two non-overlapping neuronal entities (Xu et al., 2010; Tasic et al., 2016). Thus, we injected AAV DIO *ChR2-mCherry* into M1 of *PV^{Cre}* mice, and, indeed, we detected labeled axons in the dorsal striatum that branched preferentially ventro-laterally (in 12 of 17 injected hemispheres). In contrast, injections into M2 of *PV^{Cre}* mice were less likely to result in labeled striatal projections (5 of 12 injections), and projections—when present—were sparser than the ones detected after M1 injections. Thus, for a more detailed analysis of innervation patterns, we focused on projections from M1. We injected AAV DIO *ChR2-mCherry* into M1 of *PV^{Cre}*/DRD1a-EGFP or *PV^{Cre}*/DRD2-EGFP mice (Figure 3A) and found that 31% of dSPNs, 6% of iSPNs, and 6% of cholinergic and 0% of GABAergic interneurons responded to photostimulation of M1 PV$^+$ neuron projections (Figures 3B and 3C). Thus, PV$^+$ projecting neurons preferentially innervated dSPNs (Fisher's exact test; dSPNs versus iSPNs: p = 0.009, dSPNs versus cholinergic: p = 0.04, iSPNs versus cholinergic: p = 1; Figure 3B). SPNs targeted by M1 PV$^+$ projecting neurons had a response amplitude comparable with that following stimulation of M1 SOM$^+$ projections (Figure S3C; Table S4). We verified the GABAergic nature of PV$^+$ projections to the dorsal striatum pharmacologically. Although responses could not be blocked by CNQX/D-AP5 (although one of five cells showed a clear decrease in amplitude), subsequent application

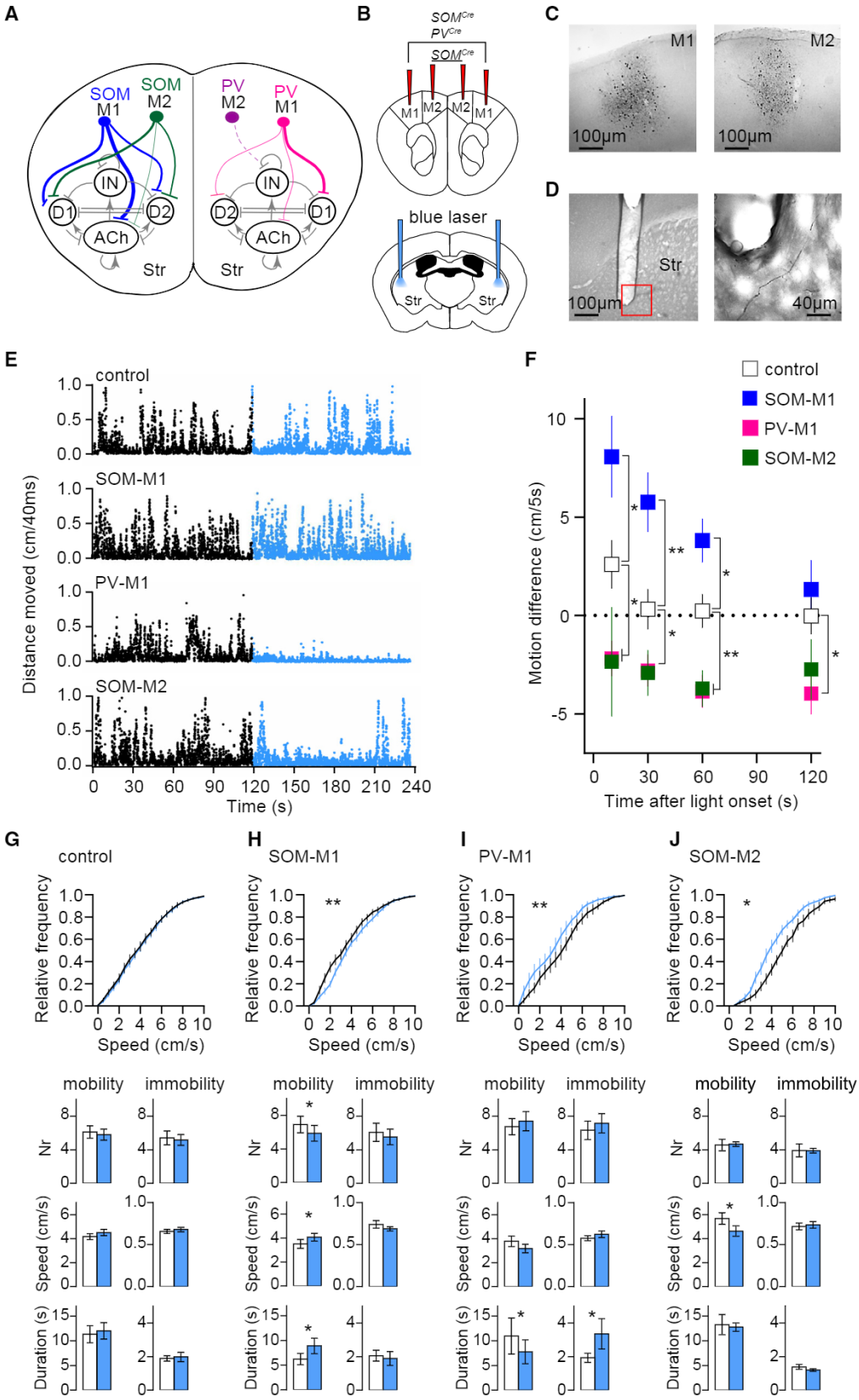

(legend on next page)

of gabazine led to a significant amplitude decrease (68.9 [147.3] pA baseline versus 70.3 [86.1] pA with CNQX/D-AP5 versus 0.5 [3.2] pA with gabazine, Friedman test, p = 0.02, post hoc Conover's test with Bonferroni correction, baseline versus CNQX/D-AP5: p = 1, baseline versus gabazine: p = 0.004, CNQX/D-AP5 versus gabazine: p = 0.009, n = 5 cells in 4 mice; Figure 3D; Figures S3G and S3H). The reversal potential of the responses was −60.3 ± 2.5 mV (mean ± SEM, n = 4 cells in 4 mice; Figure S3B; Table S4), reconfirming the GABAergic nature. SPNs targeted by M1 PV^+ projecting neurons were located 0.6 (0.7) mm posterior to the bregma, 3.0 (0.6) mm lateral, and 3.7 (0.8) deep (median [IQR]) (Figure 3E; Figures S3D–S3F; Table S4).

The different innervation patterns of SOM^+ and PV^+ projecting neurons suggested that the two cell types represent distinct subpopulations in the motor cortex. We hence analyzed whether the firing pattern of PV projecting neurons differed from that of SOM^+ projecting neurons and resembled that of "classical" PV^+ interneurons. The detection of projecting neurons was assisted by retrograde tracing with SADΔG-EGFP(EnvA) rabies virus injections into the striatum of PV^{Cre} mice expressing Cre-dependent TCB in motor cortex neurons. Indeed, all TCB^+/RbV-$EGFP^+$ non-pyramidal neurons in the motor cortex exhibited a fast spiking firing pattern with faster action potentials than SOM^+ projecting neurons (Figures 3F–3H; Figure S3I; Table S2).

Motor Cortex Long-Range Projecting SOM^+ and PV^+ Neurons Modulate Locomotor Activity

To investigate the behavioral effect of activating the newly discovered motor cortex SOM^+ and PV^+ projecting neurons (striatal targeting is summarized in Figure 4A), we implanted optic fibers bilaterally into the dorsal striatum of PV^{Cre} and SOM^{Cre} mice that were injected with AAV DIO *ChR2-mCherry* into the motor cortex (Figures 4B–4D). We compared the performance of four groups of animals: PV^{Cre} mice injected in M1 (PV-M1), SOM^{Cre} mice injected in M1 (SOM-M1), SOM^{Cre} mice injected in M2 (SOM-M2), and control mice (PV^{Cre} and SOM^{Cre} mice injected in M1 or M2 with AAV DIO *eYFP* and wild-type mice injected in M1 or M2 with AAV *Tomato*). We first asked whether activation of motor cortex PV^+ and SOM^+ neuron projections in the striatum modulated spontaneous locomotion. Mice were allowed to explore a circular arena, and locomotion was measured before and during light stimulation of corticostriatal projections (5-ms pulses at 20 Hz; power, 3 mW). We next calculated the difference between motion (defined as the distance moved in 5 s) during and before light stimulation on four epochs of different durations; i.e., 10, 30, 60, and 120 s, starting at light stimulation onset. The performance of control mice was similar before and during light stimulation (Figures 4E–4G) (the slight increase observed during the 10-s epoch was not significantly different from zero; one-sample t test (null hypothesis [H_0] = 0), $t_{(12)} = 2.1$, p = 0.06). Conversely, the performance of SOM-M1, PV-M1, and SOM-M2 changed upon photostimulation (Figures 4E and 4F). During the 10-, 30-, and 60-s epochs, SOM-M1 mice showed a significant motion increase, whereas PV-M1 and SOM-M2 mice showed a significant motion decrease with respect to control mice (Figures 4E and 4F; one-way ANOVA followed by post hoc comparisons, 10 s: $F_{(3, 31)} = 7.71$, p = 0.0005, control versus PV-M1: p = 0.03, control versus SOM-M1: p = 0.02, control versus SOM-M2: p = 0.04; 30 s: $F_{(3, 31)} = 10.48$, p = 0.0001, control versus PV-M1: p = 0.04, control versus SOM-M1: p = 0.002, control versus SOM-M2: p = 0.05; 60 s: $F_{(3, 31)} = 12.52$, p = 0.0001, control versus PV-M1: p = 0.002, control versus SOM-M1: p = 0.01, control versus SOM-M2: p = 0.008). For the 120-s epoch, only PV-M1 mice still showed a motion decrease with respect to control mice, whereas SOM-M1 and SOM-M2 performance could not be distinguished from that of control mice (Figures 4E and 4F; one-way ANOVA followed by post hoc comparisons, $F_{(3, 31)} = 3.96$, p = 0.01, control versus PV-M1: p = 0.01, control versus SOM-M1: p = 0.42, control versus SOM-M2: p = 0.13).

We characterized the photostimulation-induced motion changes occurring during the 60-s epoch in more detail. We first analyzed the cumulative frequency distribution of running speed 60 s before and for 60 s during photostimulation (Figures 4G–4J). As expected, in control mice, no difference was found between the cumulative distribution curves before and during photostimulation (Figure 4G, top; Wilcoxon matched-pairs signed-rank test, W = 193, p = 0.15). In SOM-M1 mice, the curve during photostimulation was shifted to the right, and, accordingly, the median running speed increased significantly upon photostimulation (Figure 4H, top; Wilcoxon matched-pairs signed-rank test, W = 215, p = 0.01). In PV-M1 and SOM-M2 mice, the cumulative distribution curve during photostimulation was shifted to the left, and the median running speed was significantly lower during than before photostimulation (Figures 4I and 4J, top; Wilcoxon matched-pairs signed-rank test, PV-M1: W = −113, p = 0.005; SOM-M2: W = −90, p = 0.02). Finally, based on running speed, we defined mobility and immobility bouts (Experimental Procedures) and measured their number,

Figure 4. Motor Cortex SOM^+ and PV^+ Projecting Neurons Mediate Locomotion Change

(A) Schematic drawing summarizing the newly identified corticostriatal GABAergic projections. Line thickness reflects the abundance of the distinct connections. M1 SOM^+ neurons innervate dSPNs, iSPNs, and cholinergic interneurons (blue); M2 SOM^+ neurons preferentially innervate dSPNs and iSPNs (green); M1 PV^+ neurons preferentially innervate dSPNs (pink); M2 PV^+ neuron projections are scarce (purple). D1, dSPNs; D2, iSPNs; IN, GABAergic interneuron.

(B) Schematic drawing indicating sites of AAV DIO *ChR2-mCherry* injection in SOM^{Cre} and PV^{Cre} mice (top) and of optic fiber implantation in the striatum (bottom).

(C and D) Bright-field images of DAB-stained sections showing M1 and M2 injection sites (C), optic fiber position, and mCherry-labeled axons in the striatum (D).

(E) Exemplary locomotion traces (in cm/40 ms) of control, SOM-M1, PV-M1, and SOM-M2 mice before (black) and during light stimulation (blue) (5-ms pulses delivered at 20 Hz; light power, 3 mW).

(F) Mean ± SEM difference between motion levels (in cm/5 s) during and before light stimulation for 10-, 30-, 60-, and 120-s epochs, starting at light stimulation onset.

(G–J) Mean ± SEM cumulative relative frequency of running speed (top), and mean ± SEM number, speed (in cm/s), and duration (in seconds) of mobility and immobility bouts 60 s before (black lines and white bars) and during 60-s light stimulation (blue lines and bars) for control mice (G) and SOM-M1 (H), PV-M1 (I), and SOM-M2 (J) mice. Control, n = 13 mice; SOM-M1, n = 7 mice; PV-M1, n = 9 mice; SOM-M2, n = 6 mice.

speed, and duration before and during photostimulation. In control mice, the properties of mobility and immobility bouts did not change upon photostimulation (Figure 4G; paired t test, number of bouts (nr) mobility: $t_{(12)} = 0.76$, $p = 0.46$; speed mobility: $t_{(12)} = 1.33$, $p = 0.21$; nr immobility: $t_{(12)} = 0.51$, $p = 0.62$; speed immobility: $t_{(12)} = 0.64$, $p = 0.53$; Wilcoxon matched-pairs signed-rank test: duration mobility: $W = -19$, $p = 0.54$; duration immobility: $W = -6$, $p = 0.83$). In SOM-M1 mice, photostimulation elicited significant changes in mobility bouts: the number decreased, whereas the speed and duration increased (Figure 4H; paired t test: nr: $t_{(6)} = 3.17$, $p = 0.02$; speed: $t_{(6)} = 2.97$, $p = 0.02$; Wilcoxon matched-pairs signed-rank test, duration: $W = -21$, $p = 0.03$). Immobility bouts remained unaffected (Figure 4H; paired t test: nr: $t_{(6)} = 1.46$, $p = 0.19$; speed: $t_{(6)} = 0.97$, $p = 0.37$; Wilcoxon matched-pairs signed-rank test, duration: $W = 9$, $p = 0.44$). In PV-M1 mice, the duration of mobility bouts decreased significantly, and the duration of immobility bouts increased significantly upon photostimulation (Figure 4I; Wilcoxon matched-pairs signed-rank test, duration mobility: $W = 35$, $p = 0.04$, duration immobility: $W = -39$, $p = 0.02$), whereas their number and speed remained unchanged (Figure 4I; paired t test: nr mobility: $t_{(8)} = 0.97$, $p = 0.36$; speed mobility: $t_{(8)} = 1.57$, $p = 0.14$; nr immobility: $t_{(8)} = 1.62$, $p = 0.19$; speed immobility: $t_{(6)} = 0.78$, $p = 0.46$). In SOM-M2 mice, the speed of mobility bouts was significantly reduced upon photostimulation (Figure 4J; paired t test: $t_{(5)} = 3.48$, $p = 0.02$), whereas all other variables remained unchanged (paired t test: nr mobility: $t_{(5)} = 0.14$, $p = 0.89$; nr immobility: $t_{(5)} = 0.03$, $p = 0.97$; speed immobility: $t_{(5)} = 0.26$, $p = 0.8$; Wilcoxon matched-pairs signed-rank test, duration mobility: $W = 1$, $p = 0.99$; duration immobility: $W = 11$, $p = 0.31$). In sum, we conclude that stimulation of striatal long-range projections of M1 SOM^+ neurons increased locomotion by increasing the duration and speed of mobility bouts, that stimulation of striatal long-range projections of M1 PV^+ neurons reduced locomotion by increasing the duration of immobility bouts, and that stimulation of striatal long-range projections of M2 SOM^+ neurons reduced locomotion by decreasing the speed of mobility bouts.

It has been proposed that movement control and reinforcement coding are mediated by common corticostriatal circuits (Kravitz and Kreitzer, 2012). Thus, we next asked whether stimulation of motor cortex PV^+ and SOM^+ neuron projections in the striatum also affect reinforcement/punishment coding. We tested the mice in a place preference task (Figure S4). The task lasted 3 days, during which we recorded the time mice spent in each compartment. During the first and second days (habituation and baseline, respectively), place preference was measured without photostimulation. During the third day (test), one of the compartments (stimulation side) was paired with photostimulation (5-ms pulses at 20 Hz; power, 3 mW), and place preference was measured. We calculated a difference score as the percentage of time spent on the "stimulation" side during baseline minus the percentage of time spent on the same side during the test. We found that the difference score obtained for PV-M1, SOM-M1, and SOM-M2 mice was similar to that of control mice (Figure S4B; one-way ANOVA: $F_{(3,21)} = 0.67$, $p = 0.58$). Hence, stimulation of striatal long-range projections of motor cortex PV^+ and SOM^+ neurons did not elicit place preference by employing this paradigm.

DISCUSSION

Here we show that distinct long-range GABAergic neurons connect M1 and M2 with the dorsal striatum. The newly identified long-range GABAergic neurons express either SOM or PV and differ with respect to target cell preference and the modulatory effect on motor activity.

Our results indicate that both M1 and M2 harbor long-range GABAergic neurons that target the dorsal striatum and thus extend recent findings by Rock et al. (2016). Furthermore, we report the following new findings. First, M1 and M2 contribute differentially to GABAergic corticostriatal projections. Second, we identified and characterized an additional projection formed by PV^+ neurons that differs significantly from that formed by SOM^+ neurons. And third, we demonstrate that these corticostriatal GABAergic projections modulate behavior. Multiple reasons can explain why these connections have not been noticed until recently (Rock et al., 2016). First, the scarcity of long-range GABAergic neurons constitutes a challenge as to their detection by anterograde or retrograde labeling, considering the high number of excitatory neurons that are also labeled in the same area with their axons extending along a similar path. Second, most studies focused on more dorso-anterior areas of the striatum. Hence, retrograde tracer injections are unlikely to reveal GABAergic projecting neurons in motor cortices because their axons target preferentially more lateral, posterior, and ventral parts of the dorsal striatum. However, Jinno and Kosaka (2004) did not detect motor cortical long-range GABAergic neurons even though injections included target areas that were innervated in our study. A possible reason may be low uptake efficiency and transport of the tracer FluoroGold in GABAergic neurons.

We confirmed the existence of GABAergic corticostriatal projections employing several approaches. First, there was robust axon labeling in the striatum even with regionally restricted minimal anterograde injections. Second, long-range GABAergic neurons were retrogradely labeled with CTB from the striatum. Third, long-range GABAergic neurons were transsynaptically retrogradely labeled with rabies virus that infected only striatal starter cells. Finally, the electrophysiological and pharmacological results provide strong evidence for the GABAergic nature of PV^+ and SOM^+ projecting neurons. Although we have no indication for any glutamatergic inputs deriving from SOM^+ cells, based on our immunocytochemistry, pharmacology, and rabies virus tracing, we cannot exclude that glutamatergic transmission has a minor contribution to the behavioral effects seen upon stimulation of striatal long-range projections from M1 PV^+ neurons.

It is important to note that the number of long-range GABAergic neurons presented in this study remains an underestimation because quantitative evaluations are currently hampered by a number of technical constraints. First, experiments entail "conservative/limited" virus injection to prevent viral spread beyond the target area. Second, labeling by retrograde tracing is strongly dependent on the tracer and cell type; e.g., PV^+ neurons could be detected following transsynaptic virus-mediated tracing but not by CTB labeling. For quantitative studies, it would be highly desirable to identify markers/promoters for long-range GABAergic neurons.

Characterization of motor cortex GABAergic projecting neurons revealed that M1 and M2 SOM$^+$ and PV$^+$ cells differentially innervate striatal neurons. Moreover, bilateral stimulation of corticostriatal long-range GABAergic projections modulates motor activity in spite of the scarcity of GABAergic corticostriatal neurons and the relatively small amplitude responses of targeted striatal neurons. Thus, stimulation of M1 SOM$^+$ neuron projections, targeting dSPNs, iSPNs, and cholinergic cells, leads to an increase in locomotion. In contrast, stimulation of M2 SOM$^+$ neuron projections, targeting preferentially dSPNs and iSPNs, and of M1 PV$^+$ neuron projections, targeting preferentially dSPNs, leads to a decrease in locomotion. Decreased locomotion upon preferential inhibition of dSPNs (PV-M1) is in line with previous studies showing either bradykinesia upon deletion of dSPNs (Drago et al., 1998) or increased locomotion upon stimulation of dSPNs (Kravitz et al., 2010). Notably, there was a similar effect on locomotion upon preferential inhibition of dSPNs (PV-M1) or of both dSPNs and iSPNs (SOM-M2). Comparable effects were also reported when optogenetically silencing either dSPN or both dSPNs and iSPNs (Tecuapetla et al., 2014). Increased locomotion upon stimulation of M1 SOM$^+$ neuron projections most likely reflects the participation of a larger fraction of cholinergic cells. These striatal interneurons, constituting 1%–3% of all striatal neurons, are tonically active and provide powerful feedforward inhibition to SPNs (English et al., 2011; Nelson et al., 2014), modulate corticostriatal synapses (Calabresi et al., 1998; Higley et al., 2009), and enhance dopamine release (Threlfell et al., 2012). Direct activation or inhibition of cholinergic striatal interneurons in the dorsal anterior striatum had no effect on locomotor activity (Maurice et al., 2015). However, based on our results, it is tempting to speculate that cholinergic cells in more ventral and posterior striatal areas receiving input from M1 SOM$^+$ neurons are involved in motor control. At present, we cannot resolve whether the observed change in locomotor activity results from long-range axon activation in the striatum only or whether activation of putative collaterals via back-propagating action potentials also plays a role. In either case, our results show that the activity of SOM$^+$ and PV$^+$ projecting neurons in the motor cortex differentially modulates locomotor activity. This study is also relevant when interpreting data regarding silencing of cortical areas by manipulating GABAergic neurons because the effects may also involve long-distance targets.

It has been proposed that motor control and reward coding are mediated by common corticostriatal circuits (Kravitz and Kreitzer, 2012). Our data indicate that, although activation of motor cortex PV$^+$ and SOM$^+$ neuron projections in the dorsal striatum affected locomotor activity, it did not affect place preference, although we cannot exclude their implication in reward coding more generally. On the other hand, stimulation of GABAergic projections from the prefrontal cortex to the ventral striatum induces avoidance behavior, suggesting that they are involved in the coding of punishment (Lee et al., 2014). Locomotion modulation was not addressed in the latter study. Further experiments will be required to elucidate whether, and, if so, which, corticostriatal GABAergic projections mediate both locomotion and reward coding.

This study adds to the increasing evidence that long-range GABAergic neurons are more frequent than previously thought. The heterogeneity of long-range GABAergic neurons described here is in line with previous studies indicating neurochemical diversity of long-range GABAergic neurons in the cortex and hippocampus (Jinno et al., 2007; Higo et al., 2007; Lee et al., 2014; Tomioka et al., 2005; Tomioka and Rockland, 2007). Notably, we demonstrate that distinct long-range GABAergic neurons exhibit specific functional properties and differential connectivity.

Finally, it will be of interest to study long-range GABAergic neurons in the context of movement disorders that are thought to be caused by an imbalance of dSPN and iSPN activity. Thus, parkinsonian-like movements can be reproduced by increased iSPN activity (Kravitz et al., 2010) and can be reduced by selective inhibition of striatal cholinergic interneurons (Maurice et al., 2015). Huntington's disease is marked by an early degeneration of iSPNs (Vonsattel et al., 1985; Mitchell et al., 1999) and an imbalance of excitation and inhibition of dSPNs and iSPNs (André et al., 2011). In light of our findings, it is tempting to speculate that motor cortex GABAergic projections to the striatum might be a potential target for restoring the balance of striatal output.

EXPERIMENTAL PROCEDURES

More detailed information is available in the Supplemental Experimental Procedures.

All experiments were performed in 8- to 20-week-old male mice and were approved by the Regierungspräsidium Karlsruhe in compliance with the European Guidelines for the Care and Use of Laboratory Animals (licenses G74/13 and G248/14).

Intracranial Injections and Optic Fiber Implantation

For anterograde tracing experiments, in vitro patch-clamp recordings, and behavioral experiments, AAV DIO *ChR2-mCherry* was injected into the primary and/or secondary motor cortex of *SOM^{Cre}* (Melzer et al., 2012), *PV^{Cre}* (Hippenmeyer et al., 2005), *PV^{Cre}*/GAD67-EGFP (Tamamaki et al., 2003), *SOM^{Cre}*/DRD1a-EGFP, *PV^{Cre}*/DRD1a-EGFP, *SOM^{Cre}*/DRD2-EGFP (Gong et al., 2003), and *PV^{Cre}*/DRD2-EGFP mice with a C57BL/6 background. For retrograde tracing experiments, CTB 647 was injected into the dorsal striatum of wild-type mice. For retrograde transsynaptic rabies virus tracing, AAV-CAG-Flex-TCB, AAV-CAG-Flex-RG, and SADΔG-EGFP(EnvA) were injected into the dorsal striatum of A2A-Cre mice. For monosynaptic retrograde rabies virus tracing, AAV-CAG-Flex-TCB was injected into the motor cortex of *SOM^{Cre}* (*Sst$^{tm2.1(cre)Zjh}$*, Jackson Laboratory) and *PV^{Cre}* mice, followed by SADΔG-EGFP(EnvA) injection into the dorsal striatum. In all cases, anesthesia was induced and maintained with isoflurane (1%–2.5%), and the virus was delivered through a small craniotomy at the appropriate coordinates by a glass micropipette. For behavioral experiments, optic fiber cannulas were bilaterally implanted into the striatum after viral injections.

Immunohistochemistry

Mice were transcardially perfused with 4% paraformaldehyde (PFA). Immunofluorescence and DAB staining were performed on sagittal and coronal brain sections using standard protocols.

FISH

Mice were deeply anesthetized with isoflurane and decapitated. Fresh-frozen 20-μm sections were stained with FISH using the RNAscope Fluorescent Multiplex kit (Advanced Cell Diagnostics).

In Vitro Patch-Clamp Recordings

Mice were deeply anesthetized with isoflurane, transcardially perfused with ~30 mL ice-cold sucrose solution, and 300-μm-thick brain sections were cut. ChR2-expressing long-range axonal fibers were stimulated with 5-ms

photostimulation (473 nm, 120 mW/mm^2 laser intensity). PSCs were measured at 0-mV holding potential (using Cs^+-based intracellular solution) or at −70-mV holding potential (using K^+-based, high Cl^- intracellular solution). For firing pattern analysis, incrementally increasing currents of 1-s duration were injected in current clamp mode starting at −50 or −200 pA. Series resistances of 37 megohm were accepted for analysis of PSCs. Stimulus delivery and data acquisition were performed using Pulse software. Data analysis was performed with MATLAB.

Behavioral Experiments

Mice were video-tracked at 25 frames/s, and their movements were subsequently analyzed using a position tracking system (Ethovision XT9, Noldus). The implanted optic fiber cannulas were connected to two optic fibers attached to a rotary joint (Doric Lenses). A patch cord connected the optic fibers to a diode-pumped, solid-state, 473-nm laser (CrystaLaser). We used a pulse generator (Master 8) and a transistor-transistor logic (TTL) control box (universal serial bus input/output [USB-IO] box, Noldus) to automatically control the photostimulation (5-ms pulses delivered at 20 Hz; laser power, 3 mW). Evaluation of locomotor activity was performed in a circular arena (40 × 40 cm) placed in a dimly lit room where mice were allowed to run freely for 21 min. After an initial 5-min acclimation phase, photostimulation started. It lasted 2 min and was repeated three times with an inter-stimulation period of 4 min.

Statistics

The Shapiro-Wilk test was used to test for normal distribution. Brown-Forsythe and F tests were used to test the homogeneity of variances. For non-pairwise comparisons, unpaired t tests (either for equal or unequal variance) or Mann-Whitney *U* tests were used. For pairwise comparisons, paired t tests or Wilcoxon matched-pairs signed-rank tests were used. Proportions were compared using Fisher's exact tests. For multiple pairwise comparisons, Friedman test followed by post hoc Conovor's tests was used. One-way ANOVA followed by Tukey's multiple comparisons tests was used to compare motion differences.

SUPPLEMENTAL INFORMATION

Supplemental Information includes Supplemental Experimental Procedures, four figures, and four tables and can be found with this article online at http://dx.doi.org/10.1016/j.celrep.2017.04.024.

AUTHOR CONTRIBUTIONS

S.M., M.G., and H.M. designed the experiments and wrote the manuscript with contributions from all authors. S.M. performed in vitro electrophysiology, analysis, immunohistochemistry, reconstructions, and retrograde tracing studies. M.G. performed behavioral experiments and corresponding analyses. D.E.K. performed control electrophysiological experiments and immunostaining. M.M. performed immunohistochemistry and virus injections. K.W.H. produced the pseudotyped rabies virus.

ACKNOWLEDGMENTS

We thank K. Deisseroth for the AAVs and B. L. Sabatini for providing AAVs, rabies virus, and FISH reagents; I. Preugschat-Gumprecht, U. Amtmann, R. Hinz, and B. Schwalm for technical assistance; E. Senkova for AAV injections and optic fiber implantations; and Byung Kook Lim for providing starting material for rabies virus production. The research was funded by European Research Council Grant FP 7 and ERC Advanced Grant 250047 (to H.M.) German Research Foundation (DFG) Grants MO432/10 (to H.M.), SFB1134 (to H.M.), and GI1157/1-1 (to M.G.), and German Ministry of Education and Research (BMBF) Grant 01GQ1003A (to H.M.).

Received: March 26, 2016
Revised: March 21, 2017
Accepted: April 9, 2017
Published: May 2, 2017

REFERENCES

André, V.M., Fisher, Y.E., and Levine, M.S. (2011). Altered Balance of Activity in the Striatal Direct and Indirect Pathways in Mouse Models of Huntington's Disease. Front. Syst. Neurosci. *5*, 46.

Bennett, B.D., and Wilson, C.J. (1999). Spontaneous activity of neostriatal cholinergic interneurons in vitro. J. Neurosci. *19*, 5586–5596.

Bolam, J.P., Hanley, J.J., Booth, P.A., and Bevan, M.D. (2000). Synaptic organisation of the basal ganglia. J. Anat. *196*, 527–542.

Calabresi, P., Centonze, D., Gubellini, P., Pisani, A., and Bernardi, G. (1998). Endogenous ACh enhances striatal NMDA-responses via M1-like muscarinic receptors and PKC activation. Eur. J. Neurosci. *10*, 2887–2895.

Cowan, R.L., and Wilson, C.J. (1994). Spontaneous firing patterns and axonal projections of single corticostriatal neurons in the rat medial agranular cortex. J. Neurophysiol. *71*, 17–32.

Drago, J., Padungchaichot, P., Wong, J.Y., Lawrence, A.J., McManus, J.F., Sumarsono, S.H., Natoli, A.L., Lakso, M., Wreford, N., Westphal, H., et al. (1998). Targeted expression of a toxin gene to D1 dopamine receptor neurons by cre-mediated site-specific recombination. J. Neurosci. *18*, 9845–9857.

English, D.F., Ibanez-Sandoval, O., Stark, E., Tecuapetla, F., Buzsáki, G., Deisseroth, K., Tepper, J.M., and Koos, T. (2011). GABAergic circuits mediate the reinforcement-related signals of striatal cholinergic interneurons. Nat. Neurosci. *15*, 123–130.

Fuchs, E.C., Neitz, A., Pinna, R., Melzer, S., Caputi, A., and Monyer, H. (2016). Local and distant input controlling excitation in layer II of the medial entorhinal cortex. Neuron *89*, 194–208.

Gertler, T.S., Chan, C.S., and Surmeier, D.J. (2008). Dichotomous anatomical properties of adult striatal medium spiny neurons. J. Neurosci. *28*, 10814–10824.

Gong, S., Zheng, C., Doughty, M.L., Losos, K., Didkovsky, N., Schambra, U.B., Nowak, N.J., Joyner, A., Leblanc, G., Hatten, M.E., and Heintz, N. (2003). A gene expression atlas of the central nervous system based on bacterial artificial chromosomes. Nature *425*, 917–925.

Higley, M.J., Soler-Llavina, G.J., and Sabatini, B.L. (2009). Cholinergic modulation of multivesicular release regulates striatal synaptic potency and integration. Nat. Neurosci. *12*, 1121–1128.

Higo, S., Udaka, N., and Tamamaki, N. (2007). Long-range GABAergic projection neurons in the cat neocortex. J. Comp. Neurol. *503*, 421–431.

Hippenmeyer, S., Vrieseling, E., Sigrist, M., Portmann, T., Laengle, C., Ladle, D.R., and Arber, S. (2005). A developmental switch in the response of DRG neurons to ETS transcription factor signaling. PLoS Biol. *3*, e159.

Jinno, S., and Kosaka, T. (2004). Parvalbumin is expressed in glutamatergic and GABAergic corticostriatal pathway in mice. J. Comp. Neurol. *477*, 188–201.

Jinno, S., Klausberger, T., Marton, L.F., Dalezios, Y., Roberts, J.D.B., Fuentealba, P., Bushong, E.A., Henze, D., Buzsáki, G., and Somogyi, P. (2007). Neuronal diversity in GABAergic long-range projections from the hippocampus. J. Neurosci. *27*, 8790–8804.

Kawaguchi, Y. (1992). Large aspiny cells in the matrix of the rat neostriatum in vitro: physiological identification, relation to the compartments and excitatory postsynaptic currents. J. Neurophysiol. *67*, 1669–1682.

Kawaguchi, Y., Wilson, C.J., Augood, S.J., and Emson, P.C. (1995). Striatal interneurones: chemical, physiological and morphological characterization. Trends Neurosci. *18*, 527–535.

Koralek, A.C., Jin, X., Long, J.D., 2nd, Costa, R.M., and Carmena, J.M. (2012). Corticostriatal plasticity is necessary for learning intentional neuroprosthetic skills. Nature *483*, 331–335.

Kravitz, A.V., and Kreitzer, A.C. (2012). Striatal mechanisms underlying movement, reinforcement, and punishment. Physiology (Bethesda). *27*, 167–177.

Kravitz, A.V., Freeze, B.S., Parker, P.R.L., Kay, K., Thwin, M.T., Deisseroth, K., and Kreitzer, A.C. (2010). Regulation of parkinsonian motor behaviours by optogenetic control of basal ganglia circuitry. Nature *466*, 622–626.

Kravitz, A.V., Tye, L.D., and Kreitzer, A.C. (2012). Distinct roles for direct and indirect pathway striatal neurons in reinforcement. Nat. Neurosci. *15*, 816–818.

Lee, A.T., Vogt, D., Rubenstein, J.L., and Sohal, V.S. (2014). A class of GABAergic neurons in the prefrontal cortex sends long-range projections to the nucleus accumbens and elicits acute avoidance behavior. J. Neurosci. *34*, 11519–11525.

Marshel, J.H., Mori, T., Nielsen, K.J., and Callaway, E.M. (2010). Targeting single neuronal networks for gene expression and cell labeling in vivo. Neuron *67*, 562–574.

Maurice, N., Liberge, M., Jaouen, F., Ztaou, S., Hanini, M., Camon, J., Deisseroth, K., Amalric, M., Kerkerian-Le Goff, L., and Beurrier, C. (2015). Striatal Cholinergic Interneurons Control Motor Behavior and Basal Ganglia Function in Experimental Parkinsonism. Cell Rep. *13*, 657–666.

McGeorge, A.J., and Faull, R.L. (1989). The organization of the projection from the cerebral cortex to the striatum in the rat. Neuroscience *29*, 503–537.

Melzer, S., Michael, M., Caputi, A., Eliava, M., Fuchs, E.C., Whittington, M.A., and Monyer, H. (2012). Long-range-projecting GABAergic neurons modulate inhibition in hippocampus and entorhinal cortex. Science *335*, 1506–1510.

Mitchell, I.J., Cooper, A.J., and Griffiths, M.R. (1999). The selective vulnerability of striatopallidal neurons. Prog. Neurobiol. *59*, 691–719.

Nelson, A.B., Hammack, N., Yang, C.F., Shah, N.M., Seal, R.P., and Kreitzer, A.C. (2014). Striatal cholinergic interneurons Drive GABA release from dopamine terminals. Neuron *82*, 63–70.

Planert, H., Berger, T.K., and Silberberg, G. (2013). Membrane properties of striatal direct and indirect pathway neurons in mouse and rat slices and their modulation by dopamine. PLoS ONE *8*, e57054.

Rock, C., Zurita, H., Wilson, C., and Apicella, A.J. (2016). An inhibitory corticostriatal pathway. eLife *5*, 15890.

Tamamaki, N., Yanagawa, Y., Tomioka, R., Miyazaki, J., Obata, K., and Kaneko, T. (2003). Green fluorescent protein expression and colocalization with calretinin, parvalbumin, and somatostatin in the GAD67-GFP knock-in mouse. J. Comp. Neurol. *467*, 60–79.

Tasic, B., Menon, V., Nguyen, T.N., Kim, T.K., Jarsky, T., Yao, Z., Levi, B., Gray, L.T., Sorensen, S.A., Dolbeare, T., et al. (2016). Adult mouse cortical cell taxonomy revealed by single cell transcriptomics. Nat. Neurosci. *19*, 335–346.

Tecuapetla, F., Matias, S., Dugue, G.P., Mainen, Z.F., and Costa, R.M. (2014). Balanced activity in basal ganglia projection pathways is critical for contraversive movements. Nat. Commun. *5*, 4315.

Threlfell, S., Lalic, T., Platt, N.J., Jennings, K.A., Deisseroth, K., and Cragg, S.J. (2012). Striatal dopamine release is triggered by synchronized activity in cholinergic interneurons. Neuron *75*, 58–64.

Tomioka, R., and Rockland, K.S. (2007). Long-distance corticocortical GABAergic neurons in the adult monkey white and gray matter. J. Comp. Neurol. *505*, 526–538.

Tomioka, R., Okamoto, K., Furuta, T., Fujiyama, F., Iwasato, T., Yanagawa, Y., Obata, K., Kaneko, T., and Tamamaki, N. (2005). Demonstration of long-range GABAergic connections distributed throughout the mouse neocortex. Eur. J. Neurosci. *21*, 1587–1600.

Vonsattel, J.P., Myers, R.H., Stevens, T.J., Ferrante, R.J., Bird, E.D., and Richardson, E.P., Jr. (1985). Neuropathological classification of Huntington's disease. J. Neuropathol. Exp. Neurol. *44*, 559–577.

Wang, Y., Toledo-Rodriguez, M., Gupta, A., Wu, C., Silberberg, G., Luo, J., and Markram, H. (2004). Anatomical, physiological and molecular properties of Martinotti cells in the somatosensory cortex of the juvenile rat. J. Physiol. *561*, 65–90.

Weissbourd, B., Ren, J., DeLoach, K.E., Guenthner, C.J., Miyamichi, K., and Luo, L. (2014). Presynaptic partners of dorsal raphe serotonergic and GABAergic neurons. Neuron *83*, 645–662.

Wickersham, I.R., Lyon, D.C., Barnard, R.J., Mori, T., Finke, S., Conzelmann, K.K., Young, J.A., and Callaway, E.M. (2007). Monosynaptic restriction of transsynaptic tracing from single, genetically targeted neurons. Neuron *53*, 639–647.

Wilson, C.J. (1987). Morphology and synaptic connections of crossed corticostriatal neurons in the rat. J. Comp. Neurol. *263*, 567–580.

Wu, Y., Richard, S., and Parent, A. (2000). The organization of the striatal output system: a single-cell juxtacellular labeling study in the rat. Neurosci. Res. *38*, 49–62.

Xiong, Q., Znamenskiy, P., and Zador, A.M. (2015). Selective corticostriatal plasticity during acquisition of an auditory discrimination task. Nature *521*, 348–351.

Xu, X., Roby, K.D., and Callaway, E.M. (2010). Immunochemical characterization of inhibitory mouse cortical neurons: three chemically distinct classes of inhibitory cells. J. Comp. Neurol. *518*, 389–404.

Znamenskiy, P., and Zador, A.M. (2013). Corticostriatal neurons in auditory cortex drive decisions during auditory discrimination. Nature *497*, 482–485.